Electron intersubband relaxation in doped quantum wells

Paul Sotirelis
Department of Physics, University of Illinois at Urbana-Champaign, Urbana, Illinois 61801

Paul von Allmen and Karl Hess
Beckman Institute, University of Illinois at Urbana-Champaign, Urbana, Illinois 61801
(Received 10 July 1992; revised manuscript received 8 January 1993)

The intersubband relaxation time of an electron is calculated by considering electron-electron and electron-phonon (bulk LO phonon) scattering in a GaAs quantum well. The relaxation time is derived and numerically evaluated within the random-phase approximation with full multiple subband and frequency-dependent screening. The electron scattering due to the coupled system of electrons and phonons is compared with the decoupled scattering where both electron-electron and unscreened electron-phonon scattering are considered separately. It is shown that the intersubband relaxation time is heavily influenced by the electron density in the well. It is also shown that at room temperature it is necessary to use the finite-temperature dielectric function to accurately determine the intersubband relaxation time.

I. INTRODUCTION

The intersubband relaxation time of an electron in a quantum well has been the subject of recent investigations experimentally[1] and theoretically.[2,3] The goal of much of this research has been to determine the two-dimensional nature of the longitudinal-optical (LO) phonons and how that influences the intersubband (and intrasubband) relaxation time. There have been few studies that have focused on how the electron density in the quantum well affects scattering between subbands.[4,5] However, high electron densities have been linked to rapid thermalization of the electron distribution function in quantum wells, indicating a general increase in scattering with electron density.[6] The main goal of our research is to determine the electron-density dependence of the intersubband relaxation time.

The intersubband relaxation time is calculated for an electron interacting with a given thermal distribution of electrons and/or the lattice in a single GaAs quantum well. One of the best methods for determining the intersubband relaxation time involves the evaluation of the imaginary part of the electron self-energy in the random-phase approximation (RPA).[7] This method allows the inclusion of the relevant scattering mechanisms — electron-electron and electron-phonon (LO phonons) — in a prescribed and consistent way, which is complicated by the fact that they mutually interact and affect each other.[7–9] This is in contrast to considering electron-electron scattering and unscreened electron-phonon scattering separately, and summing the two contributions.

Due to the complicated form of the equations that describe the electronic screening in the RPA for a multiple subband quantum well,[10,11] various approximations such as static screening, the long-wavelength limit, the electric quantum limit, or the plasmon-pole approximation are commonplace. These approximations overly simplify or neglect either the single pair or plasmon excitations which are expected to be important for inelastic scattering. We numerically solve the screening equations in the RPA for the matrix element of the effective electron-electron interaction potential without making any of the above approximations. Also, the overlap of the wave functions is included in a form factor that is evaluated algebraically.

A number of simplifying assumptions are made concerning the quantum-well structure which is a single GaAs layer between two $Al_xGa_{1-x}As$ regions. The states of the electrons are calculated in the effective-mass approximation where the electrons are assumed to have the effective mass at the bottom of the Γ_6 conduction band for bulk GaAs. The wave functions and energies are approximated by assuming infinite barriers and ignoring any band bending. The low-frequency dielectric function of the undoped GaAs layer is approximated by that of the bulk lattice, therefore neglecting interface and confined phonon modes (the validity of this approximation is discussed in Ref. 3). The dielectric function of the lattice is assumed to fit a single oscillator model in which the longitudinal and transverse optical frequencies are considered dispersionless.[12]

In Sec. II we derive a general expression for the intersubband relaxation rate that is valid at finite temperature and can include either or both electron-electron and electron-phonon scattering. In Sec. III the intersubband relaxation time is evaluated for various electron densities, energies, and two different temperatures, and those results are discussed. In Sec. IV the results are summarized and some concluding remarks are made. All equations are given in cgs units.

II. MODEL AND EQUATIONS

A. Electronic states

The electronic states are calculated in the effective-mass approximation. The value of the effective mass that

is used throughout this paper is given by $m^* = 0.067m_e$, where m_e is the free-electron mass. The electron wave functions and energies for a quantum well of width a are approximated by the infinite barrier height values and are given by (A is the normalization area)

$$\Psi_{n\mathbf{k}}(\boldsymbol{\rho}, z) = \frac{e^{i\mathbf{k}\cdot\boldsymbol{\rho}}}{\sqrt{A}}\psi_n(z), \quad \psi_n(z) = \sqrt{\frac{2}{a}}\sin\left(\frac{n\pi z}{a}\right), \tag{1a}$$

$$E_{n\mathbf{k}} = E_n + \frac{\hbar^2(k_x^2 + k_y^2)}{2m^*}, \qquad E_n = \frac{n^2\hbar^2\pi^2}{2m^*a^2}. \tag{1b}$$

B. Lattice dispersion

The low-frequency dielectric function of undoped GaAs is necessary to represent the dielectric properties of the lattice in the absence of conduction-band electrons in the quantum well. We assume dispersionless bulk LO phonons, and a single oscillator model[12] relating four parameters, the LO-phonon frequency ω_L, the TO-phonon frequency ω_T, the high-frequency dielectric constant ϵ_∞, and the static dielectric constant ϵ_s. The lattice dielectric function is given by

$$\epsilon_{\text{latt}}(\omega) = \epsilon_\infty + \frac{(\epsilon_\infty - \epsilon_s)\omega_T^2}{\omega^2 - \omega_T^2}. \tag{2}$$

The first term in (2) is due to high-energy electronic excitations and is a constant in the energy range of interest,[7] and the second term is due to the phonons. The values used throughout this paper are $\omega_L = 5.58 \times 10^{13}$ sec^{-1}, $\omega_T = 5.14 \times 10^{13}$ sec^{-1}, $\epsilon_\infty = 10.92$, and $\epsilon_s = \epsilon_\infty(\omega_L/\omega_T)^2$.[12]

C. Screening in quasi-two-dimensional systems

The screening of a potential in a multiple subband quantum well is described by a linear system of equations[10,11] relating the frequency and wave-vector-dependent dielectric function $\epsilon_{ijnm}(\mathbf{q},\omega)$, the matrix element of the bare Coulomb potential $V_{ijkl}^{\text{Coul}}(q)$, and the matrix element of the effective interaction potential $V_{mnkl}^{\text{eff}}(\mathbf{q},\omega)$, and is given by

$$V_{ijkl}^{\text{Coul}}(q) = \sum_{mn} \epsilon_{ijnm}(\mathbf{q},\omega) V_{mnkl}^{\text{eff}}(\mathbf{q},\omega). \tag{3}$$

Equation (3) gives $V_{mnkl}^{\text{eff}}(\mathbf{q},\omega)$ and both $\epsilon_{ijnm}(\mathbf{q},\omega)$ and $V_{ijkl}^{\text{Coul}}(q)$ are defined below.

The dielectric properties of the conduction-band electrons are given by the RPA dielectric function. Intrasubband and intersubband excitations are included (both plasmon and single pair).[13] In addition to the dielectric properties of the electrons, the dielectric properties of the lattice can also be included within the RPA. This is done through the use of a total dielectric function that includes the polarizabilities of the electrons and the lattice.[8] The dielectric function $\epsilon_{ijnm}(\mathbf{q},\omega)$ for the undoped GaAs quantum well (unscreened electron-phonon scattering), the doped GaAs quantum well neglecting the phonons (electron-electron scattering), and the doped GaAs quantum well including the phonons (electron scattering due to the coupled system of electrons and phonons) is given, respectively, by

$$\epsilon_{ijnm}(\mathbf{q},\omega) = \epsilon_{\text{latt}}(\omega)\delta_{im}\delta_{jn}, \tag{4a}$$

$$\epsilon_\infty\delta_{im}\delta_{jn} - V_{ijnm}^{\text{Coul}}(q)\Pi_{mn}^0(\mathbf{q},\omega), \tag{4b}$$

and

$$\epsilon_{\text{latt}}(\omega)\delta_{im}\delta_{jn} - V_{ijnm}^{\text{Coul}}(q)\Pi_{mn}^0(\mathbf{q},\omega). \tag{4c}$$

The term $V_{ijnm}^{\text{Coul}}(q)\Pi_{mn}^0(\mathbf{q},\omega)$ gives the polarizability due to the electrons in the quantum well and is defined below by

$$\Pi_{mn}^0(\mathbf{q},\omega) = 2\sum_{\mathbf{k}} \frac{n_f(E_{m\mathbf{k}+\mathbf{q}}) - n_f(E_{n\mathbf{k}})}{E_{m\mathbf{k}+\mathbf{q}} - E_{n\mathbf{k}} - \hbar\omega - i\varepsilon}, \tag{5a}$$

$$V_{ijnm}^{\text{Coul}}(q) = \frac{2\pi e^2}{q}\int\int dz_1\,dz_2\;\psi_i^*(z_1)\psi_j(z_1) \times\exp(-q|z_1 - z_2|)\;\psi_m(z_2)\psi_n^*(z_2), \tag{5b}$$

where n_f is the Fermi-Dirac function with the chemical potential μ.

A common approximation is to assume $V_{mnkl}^{\text{eff}} \propto V_{mnkl}^{\text{Coul}}$, which is good for static screening (i.e., Thomas-Fermi). All inelastic-scattering processes are neglected in this approximation, including electron-plasmon scattering. Another common approximation is the plasmon-pole approximation in which the plasmon and pair excitations are approximated by an effective plasmon excitation. We make no approximation in solving the linear system; in all our calculations V_{mnkl}^{eff} is determined by directly solving the linear system [Eq. (3)] by numerical methods.

D. Intersubband relaxation time

The energy broadening of a state $\mathbf{k}$ in subband i due to the electron-electron and electron-phonon interaction is described by the spectral function[7]

$$A_i(\mathbf{k}, E) = -2\,\text{Im}\,[G_{ii}(\mathbf{k}, E)]\,. \tag{6}$$

The dressed Green function in subband i, $G_{ii}(\mathbf{k}, E)$, is determined from the Dyson equation[7]

$$G_{ij} = G_i^0\delta_{ij} + G_i^0\sum_n \Sigma_{in}G_{nj}, \tag{7}$$

where the RPA self-energy, Σ_{in}, is given by

$$\Sigma_{in}(\mathbf{k}, i\omega_n) = -\frac{1}{\beta}\sum_{\mathbf{q}}\sum_{\nu_m}\sum_j V_{jinj}^{\text{eff}}(\mathbf{q}, i\nu_m) \times G_j^0(\mathbf{k}-\mathbf{q}, i\omega_n - i\nu_m). \tag{8}$$

The frequencies $i\omega_n$ and $i\nu_m$ are the standard Fermi and Bose imaginary frequencies. The function $G_j^0(\mathbf{k},\omega)$ is the Green function for a noninteracting electron in subband j and is given by[7]

$$G_j^0(\mathbf{k},\omega) = \frac{1}{\hbar\omega - E_{j\mathbf{k}} + \mu}. \tag{9}$$

The solution of Eq. (7) in matrix notation is written as

$$\mathbf{G} = (\mathbf{G}^{0\,-1} - \mathbf{G}^0\boldsymbol{\Sigma}\mathbf{G}^{0\,-1})^{-1}. \tag{10}$$

If the energy broadening is described by Eqs. (6) and (10) it is not possible to characterize it with a single relaxation rate parameter as is desired for a simple understanding of the physical process. In Appendix A we show that a simple approximate expression is obtained for G_{ii} if the nondiagonal elements of the self-energy are small compared to the energy separation between the subbands:

$$G_{ii}(\mathbf{k},\omega) = \left[\hbar\omega - E_{i\mathbf{k}} + \mu - \Sigma_{ii}(\mathbf{k},\omega) - {\sum_n}' \frac{|\Sigma_{in}(\mathbf{k},\omega)|^2}{\hbar\omega - E_{n\mathbf{k}} + \mu - \Sigma_{nn}(\mathbf{k},\omega)}\right]^{-1}. \tag{11}$$

The primed sum extends only over the subbands with the same symmetry as subband i. This restriction is due to the spatial inversion symmetry of our quantum well (see Appendix A). We see in Eq. (11) that the energy dependence of the self-energy influences the shape of the spectral function. This effect was shown to be important especially for occupied subbands.[14] However, for the range of densities under consideration, the state from which the electron scatters (subband 3) has either a zero (zero-temperature) or a very low (room-temperature) occupation probability. Therefore, we introduce a commonly used approximation and replace the energy argument of the self-energy by the energy of the noninteracting electron. We also assume that the maximum of the spectral function is still close to the peak position obtained when the nondiagonal elements of the self-energy are neglected (i.e., $\hbar\omega_{\max} = E_{i\mathbf{k}} - \mu + \mathrm{Re}[\Sigma_{ii}(\mathbf{k}, E_{i\mathbf{k}} - \mu)]$) and replace the energy in the last term of the denominator of Eq. (11) by this value. With these approximations the spectral function is a Lorenztian centered near $\hbar\omega_{\max}$ and the half-width at half height $\gamma_i(\mathbf{k})$ is given by

$$\gamma_i(\mathbf{k}) = -\mathrm{Im}\Sigma_{ii}(\mathbf{k},E) - {\sum_n}' |\Sigma_{in}(\mathbf{k},E)|^2 \frac{\mathrm{Im}\Sigma_{nn}(\mathbf{k},E)}{[E_{i\mathbf{k}} + \mathrm{Re}\Sigma_{ii}(\mathbf{k},E) - E_{n\mathbf{k}} - \mathrm{Re}\Sigma_{nn}(\mathbf{k},E)]^2 + [\mathrm{Im}\Sigma_{nn}(\mathbf{k},E)]^2} \tag{12}$$

with $E = E_{i\mathbf{k}} - \mu$. The second term in Eq. (12) can be shown to be small because the nondiagonal elements of the self-energy are small compared with the energy separation between the subbands. Therefore we keep only the first term and define the intersubband relaxation rate by

$$\tau^{-1}_{\mathbf{k}\,i\to j} = -\frac{2}{\hbar}\,\mathrm{Im}\left[\Sigma^j_{ii}(\mathbf{k}, E_{i\mathbf{k}} - \mu)\right] \tag{13}$$

$$\Sigma^j_{ii}(\mathbf{k}, i\omega_n) = -\frac{1}{\beta}\sum_{\mathbf{q}}\sum_{\nu_m} V^{\mathrm{eff}}_{jiij}(\mathbf{q}, i\nu_m) \times G^0_j(\mathbf{k}-\mathbf{q}, i\omega_n - i\nu_m). \tag{14}$$

To perform the frequency summation in Eq. (14) we use the spectral representation for $V^{\mathrm{eff}}_{jiij}(\mathbf{q}, i\nu_m)$:

$$V^{\mathrm{eff}}_{jiij}(\mathbf{q}, i\nu_m) = \frac{1}{\epsilon_\infty} V^{\mathrm{Coul}}_{jiij}(q) - \frac{1}{\pi}\int_{-\infty}^{\infty} dE\, \frac{\mathrm{Im}V^{\mathrm{eff}}_{jiij}(\mathbf{q}, E/\hbar)}{i\hbar\nu_m - E}. \tag{15}$$

In Appendix B we show how this result is obtained if V^{eff}_{jiij} is defined by Eq. (3). The frequency summation is evaluated by the standard method[7] and the resulting intersubband relaxation rate is given by

$$\tau^{-1}_{\mathbf{k}\,i\to j} = \frac{2\pi}{\hbar}\frac{2}{(2\pi)^2}\int d^2q\, \frac{1}{2\pi}\mathrm{Im}\left[-V^{\mathrm{eff}}_{jiij}(\mathbf{q},\omega)\right] \times [1 - n_f(E_{i\mathbf{k}} - \hbar\omega) + n_b(\omega)], \tag{16}$$

where $\hbar\omega = E_{i\mathbf{k}} - E_{j\mathbf{k}-\mathbf{q}}$ and $n_b(\omega)$ is the Bose statistics factor. We note that Eq. (16) includes all possible intersubband and intrasubband electronic excitations as can be seen from Eq. (3).

There is an interesting test that can be performed on the validity of Eq. (16). The intersubband relaxation rate for an electron scattering from one subband to another by emitting or absorbing a bulk LO phonon is well known and is given by[15]

$$\tau^{-1}_{\mathbf{k}\,i\to j} = \frac{e^2\omega_L}{2}\left(\frac{1}{\epsilon_\infty} - \frac{1}{\epsilon_s}\right)[n_b(\omega_L) + \tfrac{1}{2} \pm \tfrac{1}{2}] \times \int d^2q\, \frac{F_{jiij}(q)}{q}\,\delta(E_{j\mathbf{k}+\mathbf{q}} - E_{i\mathbf{k}} \pm \hbar\omega_L). \tag{17}$$

The plus is for emission and the minus is for absorption, the factor e is the electronic charge, and $F_{jiij}(q) = V^{\mathrm{Coul}}_{jiij}(q)/(2\pi e^2/q)$. Equation (16) is indeed equivalent to Eq. (17) when the electron density goes to zero, and the dielectric function used is given by Eq. (4a). This confirms that the electron-phonon scattering is correctly included.

Another correctness check on the rate from Eq. (16) can be obtained for the limiting case of electron-electron scattering with the dielectric function from Eq. (4b). This rate can be compared with the corresponding rate determined from Fermi's Golden Rule. The Fermi's Golden Rule result is given by Eq. (C4) in Appendix C. For electron-electron scattering Eqs. (C4) and (16) are almost equivalent, the only difference being the statistical factors $[n_b(\omega)+1][1-n_f(E)]$ and $[1-n_f(E)+n_b(\omega)]$. This difference is explained by decomposing the intersubband relaxation rate determined from Eq. (16) into two terms as follows:

$$\mathrm{Im}\left[-V^{\mathrm{eff}}_{jiij}(\mathbf{q},\omega)\right]\left[1-n_f(E_{j\mathbf{k}-\mathbf{q}})+n_b(\omega)\right]$$

$$=\mathrm{Im}\left[-V^{\mathrm{eff}}_{jiij}(\mathbf{q},\omega)\right]\left[1-n_f(E_{j\mathbf{k}-\mathbf{q}})\right][n_b(\omega)+1]$$
$$-\mathrm{Im}\left[-V^{\mathrm{eff}}_{ijji}(-\mathbf{q},-\omega)\right]n_f(E_{j\mathbf{k}-\mathbf{q}})n_b(\omega). \quad (18)$$

The first term yields the statistical factor and rate consistent with Fermi's Golden Rule. The physical relevance of the second term is to exclude other electrons of the same spin from scattering into the initial state $\mathbf{k}$ in subband i which is assumed to be occupied (a similar discussion is found in Ref. 7).

III. NUMERICAL RESULTS

Before the intersubband relaxation rate given by Eq. (16) is numerically evaluated, a change of variables is performed. A more suitable expression for numerical integration is arrived at by transforming the variables of integration from (q,ϕ_q) to (q,ω). This is done by introducing an energy-conserving δ function and then performing the angular integration associated with ϕ_q.[16] We assume a three-subband quantum well and evaluate the intersubband relaxation rate for transitions from subband 3 to subband 2. The quantum-well width is 220 Å and the subband energies are then $E_1 = 0.0116$ eV, $E_2 = 0.0464$ eV, and $E_3 = 0.1044$ eV (the renormalization of the subband energy through the interaction is neglected). In Sec. III A the intersubband relaxation rate due to electron-electron scattering is numerically evaluated at zero temperature using the dielectric function given by Eq. (4b). The dependence of the rate on electron energy and density is investigated. In Sec. III B the intersubband relaxation rate due to electron-electron scattering is numerically evaluated and analyzed at finite temperature (300 K). In Sec. III C the intersubband relaxation rate of an electron due to its interaction with the coupled electron-phonon system is numerically evaluated at zero temperature using the dielectric function given by Eq. (4c). The energy and density dependence is investigated and a comparison is made with the sum of the separate rates, electron-electron, and unscreened electron phonon which use the dielectric functions given by Eqs. (4b) and (4a), respectively.

A. Electron-electron scattering

The intersubband relaxation rate due to electron-electron scattering is numerically evaluated at zero temperature. In Fig. 1 the rates are plotted versus the total electron density in the well for three different initial electron energies. It is shown that at low densities the relaxation rate increases with density. At higher densities the relaxation rate reaches a maximum and then eventually decreases, the larger energy rates having their maximum rate at higher densities. When the Fermi level surpasses the energy of the second subband, the availability of the final states decreases with increasing density and therefore acts to reduce the rate. However, the decrease in the rate at high densities is only due in part to the reduction

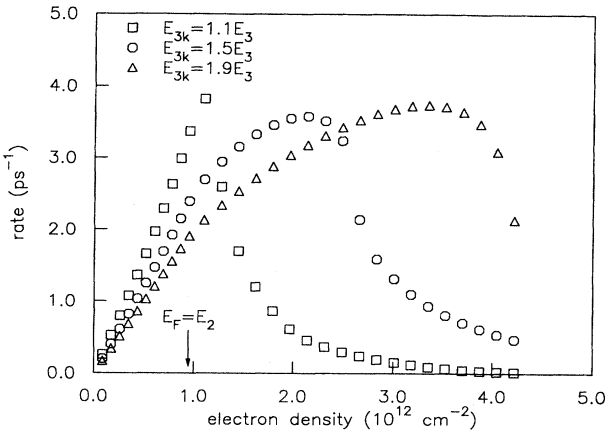

FIG. 1. Electron intersubband relaxation rate due to electron-electron scattering for transitions from subband 3 to subband 2 versus electron density for three different energies. Squares are for $E_{3\mathbf{k}} = 1.1E_3$, circles are for $E_{3\mathbf{k}} = 1.5E_3$, and triangles are for $E_{3\mathbf{k}} = 1.9E_3$. The density $n = 0.974 \times 10^{12}$ cm^{-2} is marked by the arrow and corresponds to where the Fermi level equals the energy of the second subband. The temperature is zero and the well width is 220 Å.

in the availability of final states. This is shown in Fig. 2 where the rate is calculated with and without the occupancy of final states being taken into account. In the latter case the relaxation rate still reaches a maximum and then decreases with increasing density.

The decrease in the rate at high densities is explained by examining the excitation spectrum of the electrons in the well. The plasmon dispersion is determined from

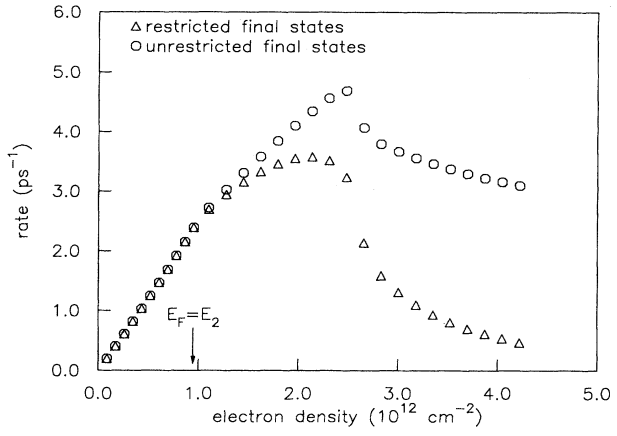

FIG. 2. Electron intersubband relaxation rate due to electron-electron scattering for transitions from subband 3 to subband 2 versus electron density with and without the final states restricted by Fermi-Dirac statistics. Triangles are for restricted final states and circles are for unrestricted final states. The density $n = 0.974 \times 10^{12}$ cm^{-2} is marked by the arrow and corresponds to where the Fermi level equals the energy of the second subband. The initial energy $E_{3\mathbf{k}} = 1.5E_3$, the temperature is zero, and the well width is 220 Å.

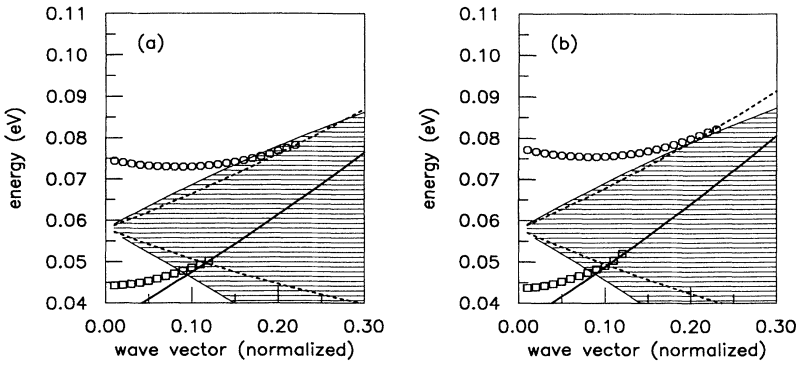

FIG. 3. Plasmon dispersion, single pair excitation region, and the region of integration for the electron densities (a) $n = 2.41 \times 10^{12}$ cm^{-2} and (b) $n = 2.74 \times 10^{12}$ cm^{-2}. The initial energy is $E_{3\mathbf{k}} = 1.5E_3$ and the wave vector is normalized to the Fermi wave vector of subband one, (a) $k_F = 3.26 \times 10^6$ cm^{-1} and (b) $k_F = 3.41 \times 10^6$ cm^{-1}. The circles and squares represent the $3 \leftrightarrow 2$ and the $2 \leftrightarrow 1$ intersubband plasmon dispersion, respectively. The dotted and solid lines represent the low wave-vector boundaries of the $3 \leftrightarrow 2$ and $2 \leftrightarrow 1$ single pair excitation regions, respectively. The shaded region is the region of integration.

the poles of $\mathrm{Im}[V^{\mathrm{eff}}_{3223}(\mathbf{q},\omega)]$ and the single pair excitation regions are where $\mathrm{Im}[V^{\mathrm{eff}}_{3223}(\mathbf{q},\omega)]$ is finite and nonzero.[17] The region of integration is determined from total energy and parallel momentum (to the layer) conservation. In Fig. 3 the plasmon dispersion and single pair excitation region are plotted along with the region of integration for densities $n = 2.41 \times 10^{12}$ cm^{-2} and $n = 2.74 \times 10^{12}$ cm^{-2} and energy $E_{3\mathbf{k}} = 1.5E_3$. It is clearly seen that at a density of approximately $n = 2.74 \times 10^{12}$ cm^{-2} and higher, emission of the $3 \leftrightarrow 2$ intersubband plasmon is forbidden by energy conservation. This is due to the increase in the $3 \leftrightarrow 2$ intersubband plasmon energy as the density increases, especially at large wave vector.

It is of interest to compare the intersubband relaxation rate due to electron-electron scattering with that of unscreened polar-optical-phonon scattering. In Fig. 4 the rates are plotted versus electron energy, and three densities are considered. At the lowest density the electron-

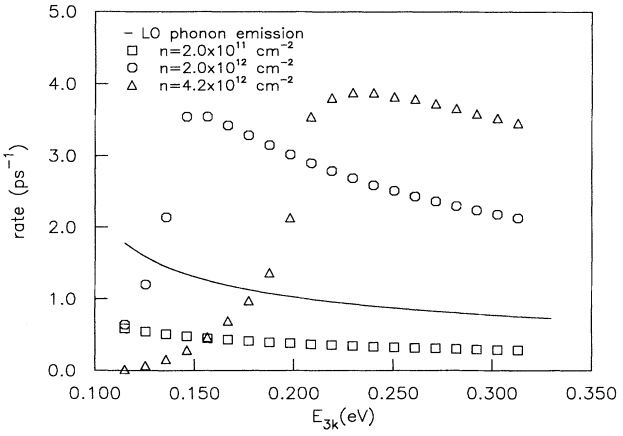

FIG. 4. Electron intersubband relaxation rate due to electron-electron scattering for transitions from subband 3 to subband 2 versus initial electron energy for three different electron densities (n). Squares are for $n = 2.0 \times 10^{11}$ cm^{-2}, circles are for $n = 2.0 \times 10^{12}$ cm^{-2}, and triangles are for $n = 4.2 \times 10^{12}$ cm^{-2}. The solid line is for unscreened LO-phonon emission. The temperature is zero and the well width is 220 Å.

electron rate is smaller than the rate for unscreened phonon emission. At higher densities the electron-electron rates can be much larger, notably at high energies. The features of Fig. 4 are explained by examining the excitation spectrum of the electrons in the well. For the density $n = 2.0 \times 10^{12}$ cm^{-2}, the sharp rise at $E \approx 0.140$ eV is due to the emission of the $3 \leftrightarrow 2$ intersubband plasmon becoming possible by energy conservation as shown in Fig. 5. Note that in the energy range under consideration, the electron energy is above threshold for the $2 \leftrightarrow 1$ intersubband plasmon. For the density $n = 4.2 \times 10^{12}$ cm^{-2} the sharp rise at $E \approx 0.200$ eV is also due to the emission of the $3 \leftrightarrow 2$ intersubband plasmon becoming possible. However, the threshold for the emission of the $2 \leftrightarrow 1$ intersubband plasmon is also at $E \approx 0.200$ eV as shown in Fig. 6.[18] Notice that in Fig. 4 the higher the density the greater the energy at which the rise occurs. This is consistent with the results of Fig. 3, where the $3 \leftrightarrow 2$ intersubband plasmon energy increases with electron density. For the electron density of $n = 2.0 \times 10^{11}$ cm^{-2} the second subband is not populated and therefore only the $2 \leftrightarrow 1$ excitations contribute. On the other hand, there is no sharp increase in the rate for this density at the threshold for $2 \leftrightarrow 1$ intersubband plasmon emission (see Fig. 4), indicating that $2 \leftrightarrow 1$ single pair excitations are the dominant scattering mechanism.

B. Finite temperature

The intersubband relaxation rate due to electron-electron scattering versus electron density is numerically evaluated at finite temperature ($T = 300$ K). Also two additional rates are numerically evaluated for comparison. The first is the corresponding zero-temperature rate where the *total* electron density is the same as in the finite-temperature calculation even though the electron density in a particular subband may be different. The second additional rate is a hybrid approximation that substitutes the zero-temperature dielectric function for the finite-temperature dielectric function. The motivation for computing these additional rates is that the electronic part of the dielectric function $\Pi^0_{mn}(\mathbf{q},\omega)$ can be reduced to an algebraic expression for zero temperature,[19]

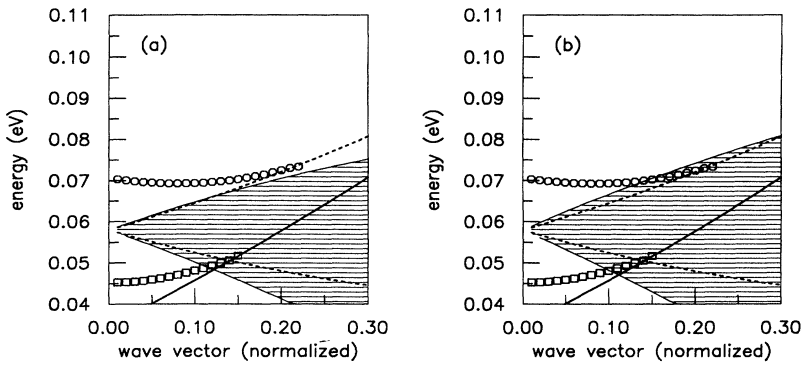

FIG. 5. Plasmon dispersion, single pair excitation region, and the region of integration for the electron density $n = 2.0 \times 10^{12}$ cm^{-2}. The electron energies are (a) $E_{3\mathbf{k}} = 0.13$ eV and (b) $E_{3\mathbf{k}} = 0.145$ eV. The wave vector is normalized to the Fermi wave vector of subband one ($k_F = 0.3029 \times 10^7$ cm^{-1}). The circles and squares represent the $3 \leftrightarrow 2$ and the $2 \leftrightarrow 1$ intersubband plasmon dispersion, respectively. The dotted and solid lines represent the low wave-vector boundaries of the $3 \leftrightarrow 2$ and $2 \leftrightarrow 1$ single pair excitation regions, respectively. The shaded region is the region of integration.

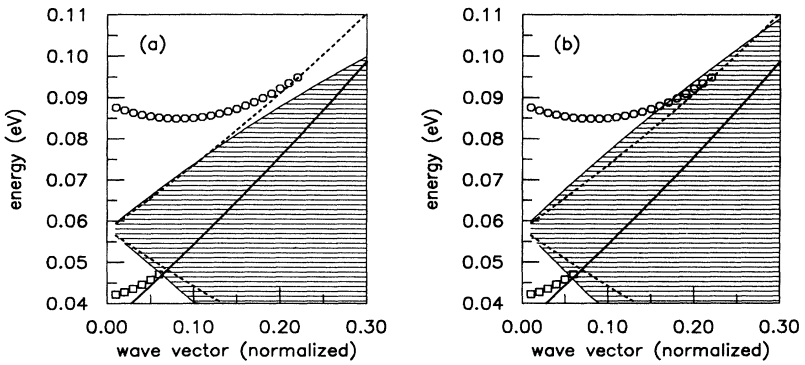

FIG. 6. Plasmon dispersion, single pair excitation region, and the region of integration for the electron density $n = 4.2 \times 10^{12}$ cm^{-2}. The electron energies are (a) $E_{3\mathbf{k}} = 0.18$ eV and (b) $E_{3\mathbf{k}} = 0.21$ eV. The wave vector is normalized to the Fermi wave vector of subband one ($k_F = 0.4039 \times 10^7$ cm^{-1}). The circles and squares represent the $3 \leftrightarrow 2$ and the $2 \leftrightarrow 1$ intersubband plasmon dispersion, respectively. The dotted and solid lines represent the low wave-vector boundaries of the $3 \leftrightarrow 2$ and $2 \leftrightarrow 1$ single pair excitation regions, respectively. The shaded region is the region of integration.

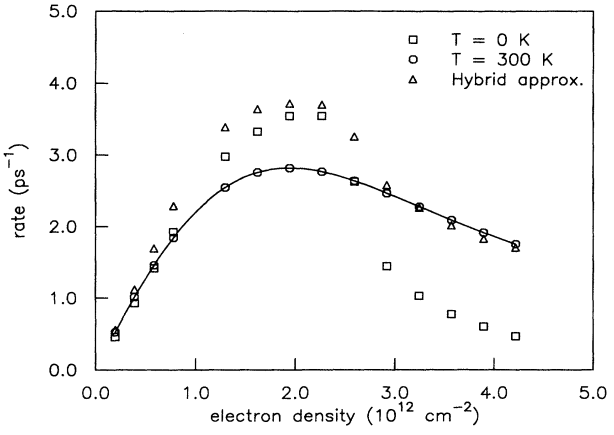

FIG. 7. Electron intersubband relaxation rate due to electron-electron scattering for transitions from subband 3 to subband 2 versus electron density for $T = 300$ K (circles), $T = 0$ K (squares), and a hybrid approximation (triangles) where the $T = 0$ K screening is used in place of $T = 300$ K screening but otherwise the full finite-temperature calculation. The initial electron energy is $E_{3\mathbf{k}} = 1.5E_3$. The solid line through the circles is a visual aid.

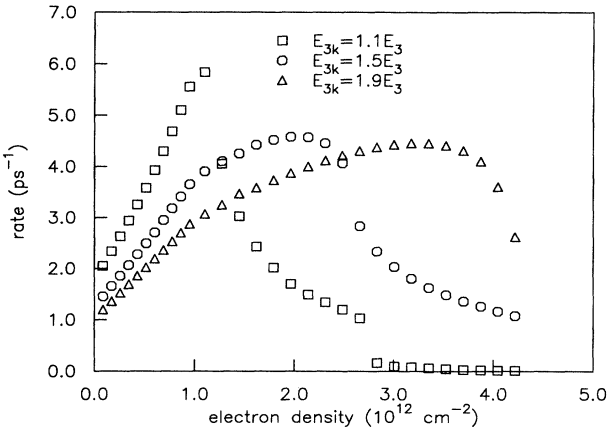

FIG. 8. Electron intersubband relaxation rate due to its interaction with the coupled electron-phonon system for transitions from subband 3 to subband 2 versus electron density. Evaluated for three different energies; squares are for $E_{3\mathbf{k}} = 1.1E_3$, circles are for $E_{3\mathbf{k}} = 1.5E_3$, and triangles are for $E_{3\mathbf{k}} = 1.9E_3$. The temperature is zero and the well width is 220 Å.

but at finite temperature the evaluation of $\Pi^0_{mn}(\mathbf{q},\omega)$ involves a numerical integration which greatly increases the computation time.

The results plotted in Fig. 7 show that the intersubband relaxation rate at zero temperature is quite different from the finite-temperature rate except at very low densities. The hybrid approximation rate is close to the finite-temperature rate only at high densities. In general there is a large range of electron densities where neither approximation agrees very well with the finite-temperature result.

C. Electron scattering from electrons and phonons

The intersubband relaxation rate of an electron due to its interaction with a coupled electron-phonon system is numerically evaluated at zero temperature using the dielectric function given by Eq. (4c). The rate is plotted versus electron density in Fig. 8 for three different initial electron energies. The general density dependence of the intersubband relaxation rate is similar to that for electron-electron scattering. At low densities the rates increase with electron density until reaching a maximum and then eventually decrease. The sudden decrease in the $E_{3\mathbf{k}} = 1.1E_3$ rate around the density $n = 2.7\times10^{12}$ cm^{-2} corresponds to the Fermi level closing to within 36 meV of $E_{3\mathbf{k}}$. Therefore the sudden decrease in the rate is due to the emission of the phonon mode becoming suppressed by Pauli exclusion.

It is of interest to compare the above rate to the rate of an electron scattering from the uncoupled electron-phonon system. The latter is the sum of the electron-electron relaxation rate [evaluated using the dielectric function given by Eq. (4b)] and the unscreened electron-phonon relaxation rate [evaluated using the dielectric function given by Eq. (4a)]. Figure 9 shows a direct comparison of the rates for energies of $E_{3\mathbf{k}} = 1.5E_3$; the rates at other energies exhibit similar behavior. At low densities the coupled and uncoupled rates agree very well, indicating that it is a good approximation to treat electron-electron scattering and electron-phonon scattering as independent scattering mechanisms. At high densities the rates due to scattering from the uncoupled electron-phonon system are consistently higher than that of the coupled electron-phonon system. This reduction in the overall coupled rate at high density indicates an increase in the mutual interactions of the electrons and the lattice (i.e., screening). Similar results have been reported for bulk GaAs.[20]

In Fig. 10 the intersubband relaxation rate of an electron due to its interaction with a coupled electron-phonon system is plotted versus energy for four different densities. The results are similar to those of Fig. 4 where only electron-electron scattering and unscreened electron-phonon scattering were considered. At the highest electron density $n = 4.2\times10^{12}$ cm^{-2} there are two regions where the rate rapidly increases. An examination of the excitation spectrum identifies these as the thresholds for emission of the $2 \leftrightarrow 1$ and $3 \leftrightarrow 2$ intersubband plasmons as shown in Fig. 11. Notice that the thresholds

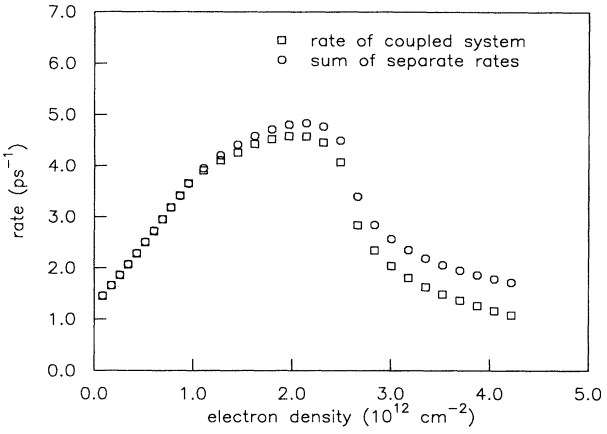

FIG. 9. Electron intersubband relaxation rate due to its interaction with the coupled and uncoupled electron-phonon system for transitions from subband 3 to subband 2 versus electron density at energy $E_{3\mathbf{k}} = 1.5E_3$. Squares and circles are for the coupled and uncoupled electron-phonon system, respectively. The temperature is zero and the well width is 220 Å.

for $2 \leftrightarrow 1$ and $3 \leftrightarrow 2$ intersubband plasmon emission no longer coincide as in Fig 4. This is a result of the modification of the $2 \leftrightarrow 1$ intersubband plasmon dispersion due to the mutual interaction of the electrons in the well and the lattice.[21] The threshold of the $3 \leftrightarrow 2$ intersubband plasmon explains the sharp rise in the rate for the density $n = 2.0\times10^{12}$ cm^{-2}. For the electron density $n = 2.0\times10^{11}$ cm^{-2}, the second subband is not populated and therefore only $2 \leftrightarrow 1$ excitations contribute. The contribution to the rate due to $2 \leftrightarrow 1$ plasmon emission is negligible, indicating that phonon and $2 \leftrightarrow 1$ single

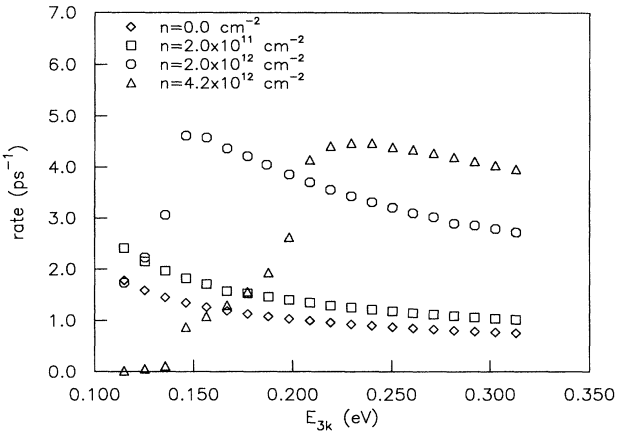

FIG. 10. Electron intersubband relaxation rate due to its interaction with the coupled electron-phonon system for transitions from subband 3 to subband 2 versus electron energy for four different densities. Diamonds are for $n = 0.0$ cm^{-2}, squares are for $n = 2.0\times10^{11}$ cm^{-2}, circles are for $n = 2.0\times10^{12}$ cm^{-2}, and triangles are for $n = 4.2\times10^{12}$ cm^{-2}. The temperature is zero and the well width is 220 Å.

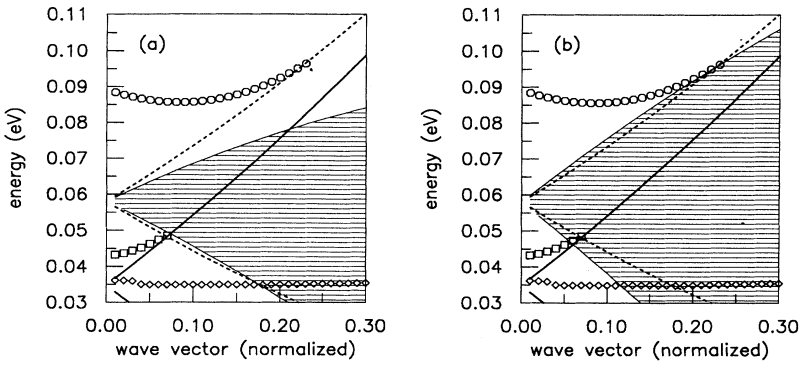

FIG. 11. Plasmon dispersion, single pair excitation regions, and the regions of integration for electron density $n = 4.2 \times 10^{12}$ cm^{-2}. The electron energies are (a) $E_{3\mathbf{k}} = 0.140$ eV and (b) $E_{3\mathbf{k}} = 0.200$ eV. The wave vector is normalized to the Fermi wave vector of subband one ($k_F = 0.4039 \times 10^7$ cm^{-1}). Circles represent the $3 \leftrightarrow 2$ intersubband plasmon dispersion. Squares represent the $2 \leftrightarrow 1$ intersubband plasmon dispersion. Diamonds represent the phonon dispersion. The dotted and solid lines represent the low wave-vector boundaries of the $3 \leftrightarrow 2$ and $2 \leftrightarrow 1$ single pair excitation region, respectively. The shaded area is the region of integration.

pair excitations dominate the scattering. The reduction in the scattering rate at low energies as the density increases indicates strong screening of the phonon modes at high densities. This is consistent with our previous result that high electron densities mutually interact with the lattice and result in screening. It is also seen that neglecting electron-electron scattering altogether is not a very good approximation even at low electron densities.

IV. SUMMARY AND CONCLUSION

The intersubband relaxation time of an electron has been determined considering electron-electron scattering and/or electron-phonon (bulk LO phonon) scattering in GaAs quantum wells. The intersubband relaxation time is derived within the random-phase approximation with full multiple subband and frequency-dependent screening. This includes numerically determining the matrix element of the effective interaction potential by solving a linear system. It should be noted that the equations are valid for the intrasubband relaxation rate as well.

The intersubband relaxation rate of an electron scattering from subband 3 to subband 2 due the conduction-band electrons in the well (coupled or uncoupled with the lattice) increases, reaches a maximum, and then decreases with electron density. The reduction of the intersubband relaxation rate at high densities is in part due to the restriction on the availability of final states and in part due to the $3 \leftrightarrow 2$ intersubband plasmon energy increasing with density. Plasmon emission plays a dominant role in the dependence of the intersubband relaxation rate on electron density and energy. At 300 K the intersubband relaxation rate substantially differs from the corresponding zero-temperature rate and the finite-temperature dielectric function is necessary to accurately determine the rate.

The relaxation rate of an electron scattering from the coupled electron-phonon system is compared with that of the uncoupled system. At low densities the coupled and uncoupled rates agree very well, indicating that it is a good approximation to treat electron-electron scattering and electron-phonon scattering as independent scattering mechanisms. At high densities the coupled rates are consistently lower than the uncoupled rates, especially at low energy, indicating that screening increases with electron density. We conclude that the effect of electron-electron scattering on the intersubband relaxation rate must be included in quantum wells at all but the lowest densities. A future direction of research could include interface and confined phonon modes since they are of interest in very thin layers and superlattices.[2,3]

ACKNOWLEDGMENTS

We would like to thank Herbert Fertig and Tetsuo Kawamura for valuable discussions. We acknowledge support from the U.S. Office of Naval Research and the National Center for Computational Electronics. Paul von Allmen also acknowledges support by the Illinois NSF Engineering Research Center.

APPENDIX A: THE G MATRIX

We want to calculate the diagonal elements of the matrix $\mathbf{G}$ given by Eq. (10). We introduce the following definitions:

$$\mathbf{B} \equiv \mathbf{G}^{-1} = \mathbf{G}^{0\,-1} - \mathbf{G}^0 \boldsymbol{\Sigma} \mathbf{G}^{0\,-1}, \tag{A1a}$$

$$B_{ii} = \Omega_i, \tag{A1b}$$

$$B_{ij} = \frac{\Omega_j}{\Omega_i} \Sigma_{ij}, \tag{A1c}$$

$$\Omega_i = \hbar\omega - E_{i\mathbf{k}} + \mu - \Sigma_{ii}. \tag{A1d}$$

The diagonal elements of the inverse matrix $\mathbf{B}^{-1}$ are given by

$$B_{ii}^{-1} = \frac{|\mathbf{B}|_{ii}}{\det(\mathbf{B})}, \tag{A2}$$

where $|\mathbf{B}|_{ii}$ is the minor for the element B_{ii}. We use the definition of the determinant

$$\det(\mathbf{B}) = \sum_{\Pi} \prod_{i=1}^{N} B_{i\Pi(i)} (-1)^P, \tag{A3}$$

where N is the order of the matrix, the sum is over the $N!$ permutations, Π is the permutation operator, and P is the order of the permutations.

In both determinants of Eq. (A2), we factorize out the product of the diagonal elements and keep only the lowest-order terms in the ratio of the nondiagonal elements of Σ to the energy separation between the sub-

bands. This approximation is based on the spectral function being sizable only at energies approximately equal to the real part of the zero of $\Omega_i(\mathbf{k},\omega)$. We then have the following expressions:

$$\det(\mathbf{B}) \cong \Omega_1 \cdots \Omega_{i-1}\Omega_{i+1} \cdots \Omega_N \left(\Omega_i - \sum_{\substack{\nu=1 \\ \nu \neq i}}^{N} \frac{|\Sigma_{i\nu}|^2}{\Omega_\nu} \right), \tag{A4}$$

$$|\mathbf{B}|_{ii} \cong \Omega_1 \cdots \Omega_{i-1}\Omega_{i+1} \cdots \Omega_N \left(1 - \frac{1}{2} \sum_{\substack{\nu,\mu=1 \\ \nu \neq \mu \neq i}}^{N} \frac{|\Sigma_{\nu\mu}|^2}{\Omega_\nu \Omega_\mu} \right). \tag{A5}$$

If we neglect the second term in $|\mathbf{B}|_{ii}$ we obtain Eq. (11). The primed sum in Eq. (11) comes from the fact that the self-energy has nondiagonal elements equal to zero between subbands with opposite parity. This follows from the fact that $V_{jinj}^{\text{Coul}} = 0$ (and therefore V_{jinj}^{eff}) if the subbands i and n have opposite parity.

APPENDIX B: SPECTRAL REPRESENTATION

We show in this appendix that a spectral representation can be written for the matrix element of the effective interaction potential in a multiple subband system. With Eqs. (3) and (4c) we can write

$$V_{ijkl}^{\text{eff}}(\mathbf{q}, i\nu_m) = \epsilon_{\text{latt}}^{-1}(i\nu_m) \left[V_{ijkl}^{\text{Coul}}(q) + \sum_{nm} V_{ijnm}^{\text{Coul}}(q) \Pi_{mn}^0(\mathbf{q}, i\nu_m) V_{mnkl}^{\text{eff}}(\mathbf{q}, i\nu_m) \right]. \tag{B1}$$

We introduce a simplified index notation with the following definition:

$$\bar{V}_{\alpha\beta}(\mathbf{q}, i\nu_m) = \epsilon_{\text{latt}}^{-1}(i\nu_m) V_{ijkl}^{\text{Coul}}(q). \tag{B2}$$

Iterating Eq. (B1) we obtain the following expression:

$$\begin{aligned} V_{\alpha\beta}^{\text{eff}} = \bar{V}_{\alpha\beta} &+ \sum_{\gamma_1} \bar{V}_{\alpha\gamma_1} \Pi_{\gamma_1}^0 \bar{V}_{\gamma_1\beta} \\ &+ \sum_{\gamma_1\gamma_2} \bar{V}_{\alpha\gamma_1} \Pi_{\gamma_1}^0 \bar{V}_{\gamma_1\gamma_2} \Pi_{\gamma_2}^0 \bar{V}_{\gamma_2\beta} \\ &+ \sum_{\gamma_1\gamma_2\gamma_3} \bar{V}_{\alpha\gamma_1} \Pi_{\gamma_1}^0 \bar{V}_{\gamma_1\gamma_2} \Pi_{\gamma_2}^0 \bar{V}_{\gamma_2\gamma_3} \Pi_{\gamma_3}^0 \bar{V}_{\gamma_3\beta} + \cdots . \end{aligned} \tag{B3}$$

Following Ref. 7, a spectral representation can be written for $V_{\alpha\beta}^{\text{eff}}$ if the energy dependence can be cast in the form

$$V^{\text{eff}}(\mathbf{q}, i\nu_m) = A(\mathbf{q}) + \sum_{\sigma} \frac{B_\sigma(\mathbf{q})}{i\nu_m - B_\sigma(\mathbf{q})}. \tag{B4}$$

With Eq. (B2), we can write the first term of Eq. (B3) as follows:

$$\begin{aligned} &\bar{V}_{\alpha\beta}(\mathbf{q}, i\nu_m) \\ &= V_{ijkl}^{\text{Coul}}(q) \frac{1}{\epsilon_\infty} \left[1 - \frac{\omega_L^2 - \omega_T^2}{2\omega_L} \left(\frac{1}{i\nu_m + \omega_L} - \frac{1}{i\nu_m - \omega_L} \right) \right], \end{aligned} \tag{B5}$$

which has the required form. The polarization function $\Pi^0(\mathbf{q}, i\nu_m)$ already has the correct form by definition [see Eq. (5a)]. The product of two or more expressions of the type of Eq. (B4) can readily be written in the same form. Therefore a spectral representation can be written for $V_{ijkl}^{\text{eff}}(\mathbf{q}, i\nu_m)$.

APPENDIX C: FERMI'S GOLDEN RULE

The intersubband relaxation rate of an electron due to only electron-electron scattering calculated at finite temperature in the RPA using Fermi's Golden Rule[16,22,23] is given by

$$\begin{aligned} \tau_{\mathbf{k}_1, i\to i'}^{-1} = \frac{2\pi}{\hbar} \sum_{\mathbf{k}_1'\mathbf{k}_2'jj'} &2 \left| V_{i'ij'j}^{\text{eff}}(\mathbf{k}_2' - \mathbf{k}_2) \right|^2 \delta_{\mathbf{k}_1' - \mathbf{k}_1 + \mathbf{k}_2' - \mathbf{k}_2} \\ &\times [1 - n_f(E_{i'\mathbf{k}_1'})] n_f(E_{j\mathbf{k}_2}) [1 - n_f(E_{j'\mathbf{k}_2'})] \delta(E_{i'\mathbf{k}_1'} + E_{j'\mathbf{k}_2'} - E_{i\mathbf{k}_1} - E_{j\mathbf{k}_2}). \end{aligned} \tag{C1}$$

The factor of 2 next to the square of the matrix element arises from the summation over three spin indices associated with the wave vectors $\mathbf{k}_2, \mathbf{k}_1', \mathbf{k}_2'$ and where the exchange terms are neglected. This expression for the intersubband relaxation time can be simplified to the following expression, where $\hbar\omega = E_{i\mathbf{k}_1} - E_{i'\mathbf{k}_1 - \mathbf{q}}$:

$$\tau_{\mathbf{k}_1, i\to i'}^{-1} = \frac{2\pi}{\hbar} \frac{2}{(2\pi)^2} \int d^2q \, [1 - n_f(E_{i\mathbf{k}_1} - \hbar\omega)] \frac{1}{2\pi} \sum_{jj'} |V_{i'ij'j}^{\text{eff}}(\mathbf{q}, \omega)|^2 \text{Im} \left[-\Pi_{j'j}^0(\mathbf{q}, \omega) \right] [n_b(\omega) + 1]. \tag{C2}$$

With an equation similar to Eq. (B3), but with $\bar{V}_{\alpha\beta}(q) = V_{ijkl}^{\text{Coul}}(q)/\epsilon_\infty$, the following identity can be derived:

$$\mathrm{Im}\left[-V^{\mathrm{eff}}_{i'iii'}(\mathbf{q},\omega)\right]=\sum_{jj'}|V^{\mathrm{eff}}_{i'ij'j}(\mathbf{q},\omega)|^2\mathrm{Im}\left[-\Pi^0_{j'j}(\mathbf{q},\omega)\right]. \tag{C3}$$

The intersubband relaxation rate is then given by

$$\tau^{-1}_{\mathbf{k}_1,i\to i'}=\frac{2\pi}{\hbar}\frac{2}{(2\pi)^2}\int d^2q\frac{1}{2\pi}\mathrm{Im}\left[-V^{\mathrm{eff}}_{i'iii'}(\mathbf{q},\omega)\right]\left[1-n_f(E_{i\mathbf{k}_1}-\hbar\omega)\right]\left[n_b(\omega)+1\right]. \tag{C4}$$

[1] D. Y. Oberli, D. R. Wake, M. V. Klein, J. Klem, T. Henderson, and H. Morkoç, Phys. Rev. Lett. **59**, 696 (1987); A. Seilmeier, H. J. Hübner, G. Abstreiter, G. Weimann, and W. Schlapp, *ibid.* **59**, 1345 (1987); M. C. Tatham, J. F. Ryan, and C. T. Foxon, *ibid.* **63**, 1637 (1989).

[2] K. Huang and B. Zhu, Phys. Rev. B **38**, 13 377 (1988); H. Rücker, E. Molinari, and P. Lugli, *ibid.* **44**, 3463 (1991); K. W. Kim and M. A. Stroscio, J. Appl. Phys. **68**, 6289 (1990).

[3] L. F. Register, Phys. Rev. B **45**, 8756 (1992).

[4] S. M. Goodnick and P. Lugli, Phys. Rev. B **37**, 2578 (1988).

[5] J. A. White and J. C. Inkson, Phys. Rev. B **43**, 4323 (1991).

[6] W. H. Knox, D. S. Chemla, G. Livescu, J. E. Cunningham, and J. E. Henry, Phys. Rev. Lett. **61**, 1290 (1988).

[7] G. D. Mahan, *Many-Particle Physics* (Plenum, New York, 1981).

[8] L. Wendler and R. Peshtedt, Phys. Status Solidi **138**, 197 (1986).

[9] R. Jalabert and S. Das Sarma, Phys. Rev. B **40**, 9723 (1989).

[10] Eric D. Siggia and P. C. Kwok, Phys. Rev. B **2**, 1024 (1970).

[11] J. Lee and H. Spector, J. Appl. Phys. **54**, 6989 (1983).

[12] J. S. Blakemore, J. Appl. Phys. **53**, R123 (1982).

[13] J. K. Jain and S. Das Sarma, Phys. Rev. B **36**, 5949 (1987).

[14] P. von Allmen, Phys. Rev. B **46**, 13 345 (1992).

[15] P. J. Price, Ann. Phys. **133**, 217 (1981); K. Yokoyama and K. Hess, Phys. Rev. B **31**, 6872 (1985); S. Das Sarma and B. Mason, Ann. Phys. **163**, 78 (1985).

[16] G. F. Giuliani and J. J. Quinn, Phys. Rev. B **26**, 4421 (1982).

[17] The $1\leftrightarrow 1$ and $3\leftrightarrow 1$ plasmon and pair excitations do not contribute to scattering and therefore are absent (because the quantum well is symmetric).

[18] The $3\leftrightarrow 2$ intersubband plasmon has a much larger contribution to the relaxation rate than the $2\leftrightarrow 1$ intersubband plasmon for the densities under consideration. This is determined by plotting $\mathrm{Im}[V^{\mathrm{eff}}_{3223}(\mathbf{q},\omega)]$ versus ω.

[19] F. Stern, Phys. Rev. Lett. **18**, 546 (1967).

[20] Ben Yu-Kuang Hu and S. Das Sarma, Phys. Rev. B **44**, 8319 (1991).

[21] The renormalization of the phonon and plasmon modes due to their interaction is small, but still shifts the threshold of the $2\leftrightarrow 1$ intersubband plasmon significantly (compare with Figs. 4 and 6).

[22] The derivation is similar to those in Refs. 23 and 16 except that in our case the electronic states given by Eqs. (1a) and (1b) are substituted for plane waves.

[23] D. Pines, *Elementary Excitations in Solids* (Benjamin/Cummings, Reading, MA, 1963).